esa

ICARUS

alpbach ICARUS

Investigating the Chronology of stellar Activity and Radiation using UV Spectra

Team Yellow:

Laura Barone, Eric Bär, Alexandre Branco, Franz de la Torre Westphal, Hülya Falkena, Zoi Filiou, Rudolf Hansen, Niklas Herzig, Valerija Koseleva, Hugo Lancery, Angelina Lonsky, Markus Maalt, Sarina Mahler, Wilhelm Öhlin, Kathryn Kennedy, Szymon Szczeciński

Tutors: Christian Gritzner & Aljona Blöcker *Cost class: M*

Abstract The *Investigating the Chronology of stellar Activity and Radiation using UV Spectra* (ICARUS) mission aims to trace the radiation history of Sun-like stars to aid the search for life outside the Solar System. So far, the majority of FGK-type stars with confirmed planets around them have not had their UV spectra characterized, which results in uncertainties in atmospheric chemistry modeling. The ICARUS mission will close this gap by measuring how the NUV stellar continuum, the Mg II emission and the Ly-α emissions of FGK-type stars change with stellar age and by analyzing their temporal emission variability. During its mission time of roughly five years, ICARUS will observe 435 targets in total, following a SSO (dawn/dusk) orbit and corresponding to an overall cost class of M. ICARUS will provide the scientific community with the first ever ultraviolet spectroscopic measurement of a systematically mapped, statistically significant, age-resolved sample of FGK-stars and will therefore aid the search for life outside the Solar System.

1 Introduction & scientific background

The search for life beyond the Solar System is guided by the premise that biospheres on other planets have developed similar environmental conditions to those on Earth. Consequently, planets orbiting Solar-type (F, G, and K) stars have become primary targets of both space- and ground-based exoplanet surveys such as *Convection, Rotation and planetary Transits* (*CoRoT*) [2], *PLAnetary Transits and Oscillations of stars* (*PLATO*) [7], and the *Very Large Telescope* (VLT) [41], as these stars are the most likely hosts of temperate, terrestrial planets with Earth-like environments. As of July 2026, there are more than 1100 known exoplanet-hosting FGK stars, which make up approximately 75% of all confirmed exoplanet host stars with known spectral types [28]. The ultraviolet (UV) radiation emitted by these stars plays a fundamental role in shaping planetary atmospheres by controlling their thermal structure and photochemistry. Moreover, stellar UV emission provides an essential observational proxy for the otherwise inaccessible extreme-ultraviolet (EUV) flux, which is the primary driver of atmospheric escape [34]. Because magnetic activity declines over time [23], the UV output of Solar-type stars evolves significantly throughout their main-sequence lifetimes, continuously modifying the radiation environment experienced by orbiting planets [8]. Understanding this evolution is therefore essential for assessing the long-term habitability of Earth-like planets. ICARUS (Investigating the Chronology of stellar Activity and Radiation using UV Spectra) aims to answer the question: How does the ultraviolet radiation environment of Solar-type stars evolve over time?

Within the UV spectrum, the Lyman-α line alone contributes approximately 37–75% of the total stellar UV flux (115–310 nm) emitted by FGK stars, depending on their level of magnetic activity. As the dominant source of UV photons, it drives much of the photochemistry in planetary atmospheres and evolves systematically with stellar age [37] [19]. The Mg II h&k resonance doublet provides a complementary diagnostic of stellar activity, serving as an empirical proxy for the EUV irradiance through its strong correlation with EUV emission [5]. Together, these spectral diagnostics trace the high-energy radiation responsible for atmospheric chemistry and escape. Despite their importance, comprehensive observations of stellar high-energy emission remain scarce. As noted by Sarah Peacock in her paper of 2025 [35], truly comprehensive coverage of the UV band remains rare. ESA's forthcoming NewAthena [27] mission will provide unprecedented X-ray observations of nearby stars, yet no comparable survey exists in the ultraviolet. The Hubble Space Telescope *Measurements of the Ultraviolet Spectral Characteristics of Low-mass Exoplanetary Systems* (MUSCLES) Treasury Survey [17] initially obtained UV spectra for only 11 nearby M and K dwarfs, excluding F and G stars, while its 2023 extension expanded the sample by just three M dwarfs, three K dwarfs, five G stars, and one F star. Consequently, no survey has yet systematically mapped the ultraviolet spectroscopic evolution of a statistically significant, age-resolved sample of FGK stars. Therefore ICARUS is designed to fill this critical observational gap, complimenting previous and future missions [29], [18], [32], [33], [15], [31], [14].

2 Science case

2.1 Science goal

ICARUS is dedicated to trace the radiation history of Sun-like stars to aid the search for life outside the Solar System, providing the missing data needed to assess the habitability of Earth-like planets. By delivering the first large, age-resolved spectroscopic survey of nearby FGK stars, ICARUS will place planetary atmosphere models on a robust empirical foundation, improving our understanding of the photochemical and escape processes driven by stellar radiation. These measurements will establish how evolving stellar UV environments influence atmospheric chemistry and the long-term potential for life beyond the Solar System.

2.2 Science objectives

In order to achieve the scientific goal, four science objectives have been formulated.

- **SO-1** – How does the Ly-α emission in FGK-type stars change with stellar age?
- **SO-2** – How does Mg II emission in FGK-type stars change with stellar age?
- **SO-3** – How does the NUV stellar continuum in FGK-type stars change with stellar age?
- **SO-4** – What is the temporal emission variability in FGK type stars?

2.3 Measurement requirements & traceability

To link the scientific objectives to the mission payload, the measurement requirements that were drawn out of the named objectives are outlined in Table 1. All the requirements listed in this table got assigned to a fitting verification column, where T means that the requirement is directly, physically testable on the instrument itself and A that the requirement is a derived parameter which is normally closed by analysis using test data as an input.

2.4 Target selection process

To determine the final target list for the mission, a step-by-step filtering process was implemented, starting from the Gaia archive [20]. For the initial selection, stars within a distance boundary of 30 pc were queried. Additionally, a restriction of single-star systems of spectral types F, G, and K has been applied. This initial step resulted in 1222 stars. Due to sensitivity constraints of our instruments, a maximum magnitude limit of 11.5 UV mag was defined. All stars that were fainter than this threshold were removed. Since the precise stellar age is crucial for the core science goals, stars lacking documented age determinations in the archive were excluded. The remaining targets were categorized by spectral type and sorted into three age groups based on [43] and displayed in Figure 1. In order to meet the mission life time requirement of 5 years, the faintest stars of each age group were removed. Within each age-sorted spectral group, the faintest targets were excluded to optimize observation efficiency. Following these steps, the selection was narrowed down to a final target list of 435 stars to be observed during the mission.

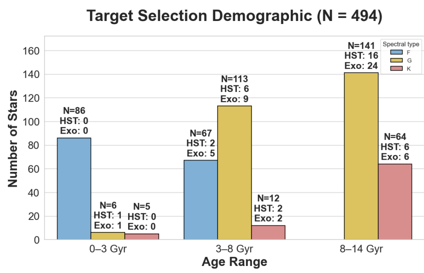

Figure 1: *Age distribution of the target stars, and the subsets observed by Hubble and known exoplanet hosts in each age bin.*

Table 1: *Requirements traceability matrix.*

Obj.	Req. ID	Requirement	Driving Parameter	Satisfied by	Verif.
SO-1	SR-010	The system shall measure 1215.67 Å with R∼10,000 for K- type stars.	R∼10,000	Ly-α spectrograph	T
SO-1	SR-011	The system shall measure 1215.67 Å with R∼40,000 for F- and G-type stars.	R∼40,000	Ly-α spectrograph	T
SO-2	SR-020	The system shall measure 2796.35 Å with R∼115,000 for all targets.	R∼115,000	Mg II spectrograph	T
SO-2	SR-021	The system shall measure 2803.53 Å with R∼115,000 for all targets.	R∼115,000	Mg II spectrograph	T
SO-1, 2, 3, 4	SR-001	The system shall record FGK-star observations with a minimum SNR of 3.	SNR of 3	All spectrographs	A
SO-1, 2, 3, 4	SR-002	The system shall be able to observe FGK-stars with a maximum UV magnitude of 11.5 at a distance of up to 30 parsec.	max UV mag = 11.5	All spectrographs	A
SO-1, 2, 3, 4	SR-003	The system shall have a pointing stability of 0.024 arcsec.	0.024 arcsec	FGS, reaction wheels	A
SO-1, 2, 3, 4	SR-004	The mission shall have a polar orbit with observing in the normal plane.	$i \sim 97.7°$	Vega-C orbit injection	A
SO-1, 2, 3, 4	SR-005	The orbit shall have a period allowing for a 5.8 min downlink window.	5.8 min downlink	Orbit and antenna(s)	A
SO-1, 2, 3, 4	SR-006	The system shall observe 435 FGK stars at least once over the mission lifetime.	435 stars	All spectrographs	A

3 Payload / instrument

3.1 Instrument sizing

The UV telescope performance was evaluated from a scaling of the Swift UVOT instrument specifications. Different apertures and exposure times were examined to identify the optimal configuration, resulting in a 0.5m aperture capable of reaching a 11.5 magnitude limit.

Table 3 compares the optical design parameters of the proposed ICARUS-UV instrument with those of the Swift Ultraviolet/Optical Telescope (UVOT) a well-characterized heritage instrument of similar wavelength range. Both instruments employ a Ritchey–Chrétien-type two-mirror configuration, with a fast primary mirror (f/2) feeding a secondary mirror that increases the effective focal ratio.

3.2 Effective Focal Length in the Two-Mirror Optical Design

Both UVOT and ICARUS-UV employ a two-mirror (Ritchey-Chrétien-type) telescope, known to be used for the UV space mission (e.g. Hubble[11]). A fast primary mirror is combined with a convex secondary mirror to achieve a long effective focal length within a compact mechanical envelope, which is also needed for this space mission.
Since the focal ratio is defined as:

$$f/\# = \frac{f_{\text{eff}}}{D}, \tag{1}$$

the effective focal length can be obtained directly from the aperture diameter D and the system's overall focal ratio. Applying this to both telescopes:

$$f_{\text{eff, UVOT}} = 0.3 \times \frac{13}{2} = 3.9 \text{ m} \tag{2}$$

$$f_{\text{eff, ICARUS-UV}} = 0.5 \times \frac{10}{2} = 5.0 \text{ m} \tag{3}$$

Even though ICARUS-UV has a faster system focal ratio (f/10 vs. f/12.7), its larger aperture gives it a longer effective focal length overall.

3.3 Selection of the System Focal Ratio

The system focal ratio was selected by cross-checking against other designs of existing and heritage UV space telescopes. Hubble (also an Ritchey–Chrétien telescope) adopt system focal ratios of the range f/12–f/13.
Given that ICARUS-UV adopts a larger aperture (0.5 m) than the UVOT/UVIT heritage instrument, the system focal ratio was therefore narrowed down from the f/12–f/13 heritage value to f/10, consistent with the precedent set by WSO-UV.

	SWIFT UVOT	ICARUS-UV
Aperture	0.3	0.5
Primary Focal ratio	f/2	f/2
System Focal ratio	f/12.7	f/10

3.4 Aperture Requirement

Longer exposure times enable detection of fainter objects, with the limiting magnitude increasing approximately linearly with the logarithm of exposure time, since SNR $\propto \sqrt{t}$ for photon-noise-limited detection. To meet the scientific requirement of SNR ≥ 3, as also noted in the SWIFT, the required integration time was calculated for the faintest stars in the target sample, yielding a worst-case total continuous observation time of approximately 4.9 years for the first observing campaign.

3.5 Payload description

The proposed payload comprises 1 telescope, 4 spectrographs, 3 dichroics, 1 tilt mirror, 1 context camera, 1 tip-tilt mirror, temperature sensors, heaters and thermal strips, all mounted on a single optical bench; the spectrographs sit on a separate optical bench. Light from the telescope passes a tilt mirror onto a first dichroic that sends > 800 nm to a VNIR context camera (doubling as the Fine Guidance Sensor) and routes < 800 nm onward through a flip mirror to the four spectrograph channels.

Table 5: *Spectrographs specification.*

Channel	Resolution	Range (nm)
Ly-α	R $\sim$ 40,000	121–122
Mg II	R $\sim$ 115,000	279–281
M-NUV	R $\sim$ 100	250–400
FUV	R $\sim$ 100	100–250

3.5.1 Mirror coating

On-axis Ritchey–Chrétien design, chosen for its compact folded geometry and for the hyperbolic mirror pair, which eliminates coma and delivers a well-corrected field. Also, mirrors are coated with Al+MgF_2, providing 80–85% reflectivity across most of the band at moderate cost and complexity, and flight-proven on Hubble, STIS, and Swift/UVOT [36].

3.6 Detector

The detector selection is driven by four constraints: high photon efficiency without filter losses, low readout noise, relaxed thermal requirements, and qualification for the mission lifetime. A microchannel plate (MCP) detector meets all four and is flight-proven on Hubble (STIS, COS) and Swift/UVOT.

A UV photon is converted to a photoelectron at the photocathode (KBr for the FUV channels, CsTe for the NUV channels, matched to each band for peak quantum efficiency and solar blindness). A double MCP stack multiplies the electron by 10^6–10^7, and the resulting charge cloud is localised on a position-sensing anode. After amplification, digitisation and centroiding, each detected photon yields position, charge and timestamp [10].

3.7 Point Spread Function

Even a perfectly figured telescope cannot image a star as a true point. Because light is a wave, diffraction at the circular aperture spreads a point source into an Airy pattern, consisting of a central lobe surrounded by concentric side lobes. The angular radius of the first minimum is given by

$$\theta_{\text{Airy}} = 1.22\,\frac{\lambda}{D}, \tag{4}$$

where λ is the wavelength and D the aperture diameter. Expressed as a physical dimension in the focal plane, this be-comes

$$\Delta x = 1.22\,\lambda\,N, \tag{5}$$

with N the system focal ratio. For ICARUS-UV ($D = 0.5$ m, $N = 10$), the Lyman-α line at 121.6 nm yields $\theta_{\text{Airy}} = 0.061''$, or 1.48 μm at the focal plane.

This wavelength dependence has a direct design consequence: a single slit geometry cannot serve all channels efficiently. The PSF therefore forms the basis for the individual slit dimensioning presented in the following section, and sets the spatial scale against which the pointing stability requirement is derived.

3.8 Slit Dimensioning

Slit width and height are sized by different criteria. The **width** governs spectral resolution: too wide degrades resolution and admits background, too narrow rejects photons. It is therefore dimensioned to the second minimum of the Airy pattern,

$$w = 2 \times 2.233\,\lambda\,N = 4.466\,\lambda\,N, \tag{6}$$

which encircles approximately 90–95% of the total flux. The **height** does not affect resolution and is sized for throughput: the PSF core in pixels plus a margin of three pixels on each side, covering residual pointing jitter and drift [44, 26, 6].

For the broadband channels the two dimensions use opposite ends of the band: the width is set by the shorter wavelength (smallest blur, tightest resolution case), the height by the longer wavelength (largest blur, avoiding clipping) [42] [22].

The Ly-α and FUV slit widths fall below the 9 μm detector pixel pitch and therefore require modest internal magnification (1.66× and 2.01×) to concentrate the flux within a single pixel. The Mg II and NUV channels need none.

4 Mission analysis & design

4.1 Design drivers

The sizing driver is photon starvation, not orbital mechanics. Reaching SNR 3 on a UV magnitude 11.5 target sets the 0.5 m aperture, and the resulting integration time which is multiplied by 435 targets sets the mission lifetime directly. Every orbital choice below protects that integration: thermal stability, stray-light exclusion and uninterrupted target visibility, rather than ground-track coverage. Secondary drivers are the ± 0.1 K payload thermal stability and the 0.024 arcsec pointing stability.

4.2 Fine Guiding System

Coarse pointing from star trackers, gyroscopes and reaction wheels achieves $\sim$10 arcsec. The FGS field of view is set to $\sim$20 arcsec, a factor of two margin, to guarantee acquisition of the target despite residual pointing uncertainty.

Fine pointing to the required 0.024 arcsec (SR7.1) is achieved by a closed feedback loop: a CMOS imager measures the stellar centroid and drives a two-axis tip–tilt mirror that corrects the beam many times per second. The imager pixels are deliberately oversampled relative to the PSF, enabling sub-pixel centroid precision well below the pointing requirement [30].

4.3 Mission phases & timeline

Table 8: *Mission phases and key activities.*

Phase	Dur.	Key activities
LEOP & comm.	1 mo.	Detumble, array and aperture-door deployment, bake-out, calibration.
Nominal science	4.9 yr	Single-campaign survey of all 435 targets. 3× re-visit of the 105 brightest for flare tracking.
Extended science	4.9 yr	Full re-observation of the sample. Variability on the timescale of years
Disposal	<5 yr	Passivation, de-orbit burn, re-entry (ESSB-ST-U-007)

The nominal phase is not an allocation but a result: it is the time needed to work through the catalogue at the observation durations given in 4.6, and is therefore fully consumed by the science plan. The extended phase repeats the survey to capture activity-cycle timescales, and drives the 10-year propellant and array sizing.

4.4 Target orbit

The baseline is a dawn/dusk Sun-synchronous terminator orbit (SSO) at 597 km. The altitude is bounded from below by drag make-up Δv and from above by the inner Van Allen belt and the peak debris flux near 800 km [24]. 597 km sits in the resulting window while keeping the ground-station pass length at 5.8 min/orbit. The terminator plane keeps the Sun permanently close to the orbit normal, which (i) allows a single anti-sun radiator to hold the ± 0.1 K payload requirement without cyclic thermal loading, (ii) permits a fixed solar-array orientation with near-continuous illumination, and (iii) maximises the fraction of the sky free of the Sun, Earth-limb and Moon exclusion cones during long integrations.

Table 9: *Launch and orbit baseline.*

Parameter	Baseline
Launcher	Vega-C, dedicated launch
Orbit type	Dawn/dusk SSO (terminator)
Altitude	597 km
Inclination	$\sim 97.7°$
Orbital period	96.62 min (15 orbits/day)
LTAN	06:00 / 18:00
Nodal drift	$\sim$1°/day (Sun-synchronous)
Transfer strategy	Direct injection, no phasing
Wet launch mass (CBE)	$\sim$984 kg
Vega-C SSO capability	$\sim$2300 kg
Launch mass margin	$\sim$1320 kg ($\sim$57%)
Fairing envelope	3.3 m dia. × >9 m
Stowed S/C envelope	2.5 × 1.1 × 1.1 m

Vega-C is oversized for the current 984 kg configuration. The large mass margin is retained deliberately at this maturity because the payload optics sit at TRL 5 and are the most likely source of mass growth.

4.5 Δv budget

Margins are set by confidence: 5% on the disposal burn, whose geometry is fixed, and 100% on the drag, desaturation and collision-avoidance allocations, whose underlying models. The solar activity across a ten-year span and wheel-momentum accumulation are weakly constrained at this stage and shall be further studied in next mission design phase.

Table 10: *Δv budget with per-phase margin.*

Phase	Δv (m/s)	**Mrg.** (%)	Δv^{+} (m/s)
Injection-dispersion corr.	10	100	20
Drag make-up (10 yr)	12	100	24
Collision avoidance	4	100	8
Wheel desaturation	3.5	100	7
Controlled de-orbit	190	5	200
Total	**219.5**		**259**

Disposal dominates the budget. The 200 m/s allocation covers lowering perigee to re-entry altitude plus finite-burn and attitude losses, and satisfies the ESA clearance rule directly rather than by decay analysis. The budget closes against SR 8.1: 115 kg of hydrazine at $I_{sp} = 220$ s delivers 268 m/s from the 869 kg dry mass, against the 260 m/s required.

4.6 Observation strategy / ConOps

4.6.1 Target selection

The 435-star catalogue (Section 2.4) is surveyed in a single campaign, one target at a time. Every target is observed at least once (SR-006); the 105 brightest are observed three times to resolve flare events on hourly timescales, which is what closes SO-4. Ideally we would have modeled the stellar variability with for example to provide better approximations on stellar variability timescales, but observing the stars spectrum consecutively seemed sufficient. The sample retains 43 confirmed exoplanet hosts and 27 stars with archival HST spectra, giving direct continuity with MUSCLES. The extended phase re-observes the full sample.

4.6.2 Orbital constraints

The ICARUS mission, distinguish itself from other mission by it's original orbit choice. Indeed, an SSO (dawn/dusk) orbit has many benefits detailed in section 4.4, which of course, will also comes with many trade-off. This is especially the case when looking at the observation strategy discussed below.

Targets are observed one at a time, inertially pointed, with the integration accumulated across successive orbits. The mission overall orbital view is composed of the Sun, the Earth, the Moon and ICARUS. The presence and interaction of these objects together around the orbit induce clear constraints in terms of visibility, treated as exclusion cones (Sun, Earth limb and Moon). The orbit altitude, set to 597km, results in a tight window to observe a given star in the sky. This is in particular the case for high declination, where the Earth limb block the view during a great amount of the integration time described in section 2.4.

To tackle this problem, we propose a preliminary approach considering the worst case possible for Earth and Moon occultation.

$$\psi_E = 2\arcsin\left(\frac{R_E + h_a}{R_E + h_s}\right) \tag{7}$$

$$\psi_M = 2\arctan\left(\frac{R_M}{d_{EM}}\right) \tag{8}$$

$$\varepsilon = \frac{\psi}{360} \tag{9}$$

With ε the occultation percentage during a single orbit at the equator looking through Earth in the equatorial plane. R_E Earth radius. R_M Moon radius. d_{EM} Earth to Moon distance. h_a the minimal height observable without perturbation from the atmosphere. h_s the satellite altitude.

Table 11: *Single orbit occultation ratio (Equatorial case)*

Body	t	ψ	ε
Earth	41 min	152.7°	42.42%
Moon	13.9 min	0.52°	0.14%

We can deduce from trivial trigonometry with ψ, the field of study angle, which shows the maximal angle to study a star without occultation while facing the sun anti-direction. We found for ICARUS, a field of study angle of $180° - \psi = 26°$. This result raised a late concern on the mission total duration, which shall be precisely characterized.

Numerical propagation of the baseline orbit shows that a 6-day (518.4 ks) integration will requires up to 9.6-days of wall-clock time once these interruptions are accounted for, a ∼42.4% penalty for only Earth and up to ∼0.13% with only Moon. For the worst observable target and worst observation condition. This is the mission's dominant schedule risk (SR-1): the 4.7-year nominal phase is sized on integration time alone, so the constraint penalty must be absorbed by observing the faint tail of the sample near solstice, when the terminator geometry opens the largest continuously visible sky region.

4.6.3 Duty cycle

Observations are accumulated across successive orbits with the spacecraft inertially pointed. The worst-case observation takes 423 ks (4.9 d) of wall-clock time; the average is 86 ks (1 d). Within each orbit the spacecraft cycles between science integration, a 5.8 min ground contact and slew-and-settle transitions at target changeover. Because the array is Sun-pointed throughout in the terminator plane, no recharge cycle interrupts science mode, and the downlink is performed without breaking inertial pointing.

Table 12: *Mission duty cycle by mode.*

Mode	**Share**
Observation	90%
Communications	4%
Manoeuvre	4%
Nominal (non-observing)	1%
De-orbit	1%

4.7 Ground segment & operations

The baseline is a single prime station, ESA Kiruna (KIR-1, 15 m, 67°51′ N / 20°57′ E), supporting S-band TT&C uplink and X-band payload downlink; the co-located 13 m KIR-2 provides back-up. The high latitude places the station inside the convergence region of the polar ground tracks, so 10–15 of the 14.9 daily revolutions produce a usable pass. The link closes with a factor of four on data volume, so communications are not a mission constraint: a missed pass is recovered on the next revolution well inside the buffer depth. Mission operations run from ESOC on CCSDS-standard services, with science operations and the archive at ESAC.

Table 13: *Ground segment and data budget closure.*

Parameter	Baseline
Prime station	ESA Kiruna KIR-1, 15 m
Back-up	Kiruna KIR-2, 13 m
S-band TT&C	2025–2110 up / 2200–2290 MHz down
X-band science	8025–8400 MHz (EESS)
Passes	10–15 of 14.9/day, 5.8 min mean
Contact time	72.5 min/day
Downlink rate	2.0 Mbit/s
Downlink capacity	0.92 GB/day
Data generated	0.23 GB/day (incl. 20% margin)
Volume margin	4.0×
Data per observation	50 MB
Buffer used / available	150 / 200 MB
Protocol	CCSDS
Operations	ESOC (mission), ESAC (science)

5 Spacecraft design & Resource budgets

5.1 Configuration & structure

The structure is sized by four requirements: survive Vega-C launch loads without resonance, retain payload alignment after launch, isolate reaction-wheel vibration from the optical bench, and keep the centre of mass on the thrust axis. The payload is isostatically mounted to decouple it from bus distortion and thermally isolated by straps and a dedicated radiator. Because UV throughput is highly sensitive to molecular and particulate contamination, an aperture door, purging and bake-out are carried, and the thrusters are oriented away from the aperture. The bus provides 5 mm of aluminium shielding, giving 10 krad tolerance over the nominal and extended mission. With the payload design fixed, the bus is built around it — structure, power, thermal control, pointing and propulsion — while preserving accommodation and alignment needs. The payload occupies 2.5 × 2.0 × 2.0 m (CBE mass 160 kg); the bus behind it adds 1.5 m stack depth, for a stowed envelope of 2.5 × 2.0 × 3.5 m. The payload sits forward-facing, isolated from bus vibration and heat; the aft bus holds the propulsion tank, wheels, avionics and batteries near the centreline to keep the centre of mass on-axis. A radiator sits on the anti-sun face, clear of the two solar wings (1.9 × 1.05 m each, 3 m² total), stowing at launch and deploying after separation. Vega-C (3.3 m fairing, >9 m tall [16] is the baselined launch vehicle; the stowed envelope, plus adapter and clearance, fits within its dynamic envelope with margin.

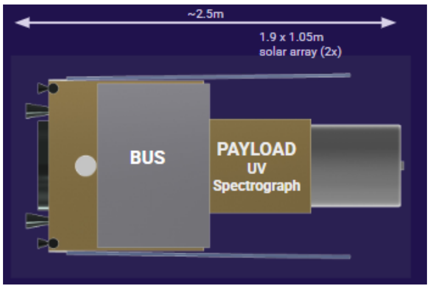

Figure 3: *Preliminary spacecraft CAD configuration (top view, not to scale).*

5.2 Propulsion

The payload (telescope, spectrographs, imager, optics) is mechanically isolated via an isostatic interface plate to prevent bus distortion. Electrical, data, and thermal interfaces connect to the OBC, EPS, and dedicated radiators. Fine guidance relies on a direct loop between the payload FGS and AOCS. To protect optical alignment and maintain high UV throughput, strict contamination controls are implemented: low-outgassing materials, aperture protection, purging, material bake-out, and plume-safe thruster placement.

5.3 Power (EPS)

The worst-case manoeuvre-mode consumption (payload + bus, after margins) is 810 W. To cover this with margin for charging, degradation and pointing losses, the array is sized to 1.4 kW BOL — giving 913 W EOL, above the 903 W worst case.

Using AZUR SPACE 3G30-class cells (30% efficiency) [1] and a real yield of 360 W/m² (90% packing factor), the array needs 3 m² for 1.05 kW BOL, split across two wings of 1.9 × 1.05 m each [9].

The dawn-dusk SSO keeps the array sun-pointed with no regular eclipse (beta 90°, clear of the 66° threshold at 600 km), removing the eclipse-cycling load a non-terminator orbit would impose. Battery sizing is instead driven by safe-mode contingency and peak-load shaving, allowing higher depth-of-discharge than an eclipse-cycled pack.

Two EnerSys ABSL CM1040 modules (28 V, 1066 Wh each, 8.8 kg) are baselined in parallel: 2132 Wh combined, covering a 12-hour safe-mode contingency with internal redundancy — losing one module still leaves the bus covered. A PCDU with max-power-point tracking distributes power, sized to the safe-mode floor.

EPS, batteries and arrays contribute 103.6 kg base mass — down from 125 kg once the battery line was resized to the dawn-dusk orbit (two CM1040 modules, 17.6 kg combined) rather than every-orbit eclipse cycling.

5.4 AOCS & pointing

Attitude determination combines a star tracker—matching observed star patterns to an onboard catalogue for absolute attitude—with gyroscopes for rapid rate sensing between updates; the AOCS estimator fuses both into a single attitude/rate estimate. During science operations, the payload-mounted Fine Guidance Sensor (FGS) measures target position in the instrument field of view, feeding the controller, which computes fine pointing error and commands the reaction wheels.

Four pyramidal reaction wheels give three-axis control with single-failure redundancy. As they saturate from secular disturbance torques, desaturation is performed periodically by the propulsion system, since no magnetorquers are carried; propulsion also handles orbit-maintenance and end-of-life manoeuvres.

Example hardware: a Sodern Hydra-family star tracker [40], space-qualified fibre-optic or MEMS gyroscopes, four pyramidal reaction wheels drawing on Bradford Space heritage [4], a fine-guidance camera, and Moog MONARC-22-6 hydrazine thrusters, configurable for desaturation and small manoeuvres [39], [3].

The AOCS/Fine Pointing system has a 44 kg base mass (46.2 kg with margin) for wheels, star trackers, and gyros/sun sensors. The OBC hosting the AOCS software is budgeted under OBC & Data Handling; propulsion hardware for desaturation is budgeted under Propulsion.

5.5 Thermal

Requirement DR3.0 (measure 1215.67 Å at R∼40,000 for F/G stars) drives the need for active thermal control to maintain optical and detector stability for high-resolution UV spectroscopy. The thermal control uses dedicated radiators, multilayer insulation (MLI), thermal straps or heat pipes and distributed temperature sensors to maintain detector thermal stability, preserving pointing, focus, spectral resolution and wavelength calibration [12].

Table 14: *Thermal control metrics.*

Parameter	Value
Passive control	MLI, radiators and/or sunshield
Active control	Sensors and controllers
Operating temperature	20 ± 0.1 °C
Total thermal mass (TBD)	∼38 kg
Heritage	CHEOPS [24]

5.6 Communications

The spacecraft bus accommodates the communications subsystem, including transmitters, receivers, amplifiers, and antennas, by managing operational power budgets and placing antennas to keep the payload aperture, payload radiator, and solar arrays unobstructed. Baselining specific flight hardware (Safran Data Systems X-NEO X-band transmitter and Honeywell STC-MS03 S-band transceiver) in place of generic heritage estimates reduced the subsystem's base mass from 30 kg to 6 kg (6.6 kg with margin) [25], [21].

Table 15: *Communication key values.*

Parameter	Value
Purpose	Science data download, TT&C and spacecraft comms
Architecture	X-band science downlink & S-band/low-rate TT&C
Key components	Transceiver (STAR EWC15-NG), RF amplifiers, antennas
Data rate	Up to ∼200 Mbps (X-band)
Mass	∼30 kg
Peak power	∼120 W (downlink mode)
Heritage	Syrlinks X-band systems, ESA mission heritage

5.7 Data handling & OBC

The communications subsystem itself; transmitters, receivers, amplifiers and antennas, is designed by the communications team; the spacecraft bus's responsibility is to accommodate it. Antennas are positioned and their fields of view chosen so that they do not obstruct the payload aperture, the payload radiator, or the deployed solar arrays, and power is allocated per operational mode (idle, downlink, uplink) from the overall power budget. The communications subsystem contributes a base mass of 6 kg (6.6 kg with margin) to the respective communications hardware. This is down from an earlier 30 kg placeholder once the comms team specified actual flight hardware (Safran Data Systems X-NEO X-band transmitter, Honeywell STC-MS03 S-band transceiver) in place of the earlier generic heritage estimate [38].

Table 16: *OBC key values.*

Parameter	Value
Spacecraft OBC	GomSpace NanoMind HP [**src-gomspace**]
Payload computer	Dedicated payload processor
OBDH storage	200 MB
Mass	∼17 kg
Science power	∼65 W
Interfaces	SpaceWire, LVDS, RS-422
Function	Command, telemetry and science data management

5.8 Mass budget

Table 1 summarises the current best-estimate spacecraft-bus mass budget by subsystem, alongside the dry-to-wet mass build-up. The dry-mass CBE of 582.5 kg (including the 159.9 kg payload) grows to a wet launch mass CBE of 983.4 kg once subsystem margins, a 30% system reserve and the 72 kg, 10-year propellant allocation are applied. The calculated mass budget is shown in 4

Subsystem	Base CBE (kg)
Payload (provided by payload team)	159.93
Structure (incl. LV adapter)	150
Thermal control (bus)	30
AOCS	44
EPS (arrays, batteries, PCDU)	103.6
Communications	6
Propulsion hardware (dry)	26
OBC & data handling	16
Other (harness, mechanisms, misc.)	50

Mass Budget:	Base CBE (kg)	With margin (kg)
Dry mass subtotal	582.54	667.98
System reserve (30%)	–	200.40
Reserved dry mass	–	868.38
Propellant (10-year, nitrogen)	–	115
Wet launch mass (CBE)	–	983.38

Figure 4: *Mass Budget*

The mass budget closes comfortably against Vega-C launch capability; final payload accommodation and structural margins remain Phase-A design drivers.

5.9 Power budget

Table 17: *Power budget by operating mode (W). Requirement includes 30% system margin and maturity margin according to ESA handbook [13]*

(W)	Idle	Op.	Man.	Sci.	Downl.	Upl.
Payload	144	144	144	249	144	144
Spacecraft	173	253	479	295	267	274
CBE demand	317	397	623	544	412	517
Req. w/ margin	412	516	**810**	707	536	673

The EPS distributes power through the PCDU, supported by the 1.05 kW BOL solar array and Li-ion battery. Maneuvering mode is the sizing case at ∼810 W after maturity, distribution-loss and system margins.

5.10 Data, link & pointing budgets

Table 18: *Data budget: generated vs downlink vs. storage.*

Parameter	Value
Orbital period	96.5 min
Orbits per day	14.9
Contact time per day	32.4 min
Link-budget ceiling (ref.)	9 Mbit/s
Selected downlink rate (EWC15-NG)	2 Mbit/s
Minimum required data rate	1.35 Mbit/s
Data generated per day	0.23 GB/day
Downlink capacity per day	0.4 GB/day
On-board storage requirement	200 MB
Buffer need (3 observations)	150 MB

6 Programmatics

6.1 Cost

Table 19: *Cost estimation (ESA CaC estimate, M-class, 2025 e.c.).*

Segment	Cost (M€)
Standard spacecraft (5 yrs)	280
Launcher + purging (Vega-C, +1 purging pass)	58
Mission operations, MOC (5 yrs nominal)	54
Science operations, SOC	44
Payload + telescope (ESA Member States)	10
Industrial margin	92
Subtotal	*538*
+25% margin	*70*
Total (CaC, 2025 e.c.)	**∼608**

The M-class cost cap lies at 670 M€ (CaC, 2025 e.c.), so the mission cost estimation lies within the class band. Payload is assumed to be provided and funded by ESA Member States.

6.2 Critical TRL & technologies

Table 20: *TRL assessment.*

Technology	TRL
Payload optics (telescope + 4 spectrographs, bespoke first-of-kind combination)	3–4
UV contamination control & bake-out	4
Custom low-CTE optical bench	5
Bus subsystems (AOCS, EPS, comms, propulsion — flight-proven heritage)	8–9
Overall mission TRL	**∼3**

Lowest-TRL items: the payload optics — the telescope and four spectrographs in their bespoke, first-of-kind combination (TRL 3–4), with UV contamination control and bake-out (TRL 4) and the custom low-CTE optical bench (TRL 5) close behind. **Development path / fallback:** UV contamination control is addressed through materials selection and thruster placement driven across the whole bus, rather than isolated to the payload, so structure, thermal, and propulsion interfaces are co-designed against a single contamination budget from the outset. The optical bench and remaining structural/harness/mechanism allocations — currently carrying a 50 kg "Other" margin — are expected to firm up as the design matures toward PDR, tightening this estimate rather than revealing new risk.

All bus subsystem hardware, by contrast, is drawn from flight-proven or modified off-the-shelf heritage (Sodern, Moog, AZUR SPACE, Bradford Space, Syrlinks), sitting at TRL 8–9. Because system-level readiness is set by the least mature science-critical element rather than an average across subsystems, the mission's overall TRL of ∼3 is driven entirely by the payload optics; the bus carries essentially none of the technology-maturation risk.

6.3 Risk register

Table 21: *Risk register: likelihood × consequence with mitigation. Prob: likelihood. Sev: severity.*

ID	Risk	Prob.	Sev.	Mitigation
SR1	Long integration times	M	M	Reduce number of targets
PR2	Internal mechanical vibrations	L	H	Test for vibrations from actuators; dampening.
PR3	Thermal control failure - risks structural warping of optics	M	H	Thermal load tests, optimize the thermal system.

All three risks fall in the yellow (medium) band of the project's 5×5 risk matrix (severity 1–5 × likelihood A–E), reflecting manageable but non-negligible exposure. PR2 and PR3 carry the higher severity of the set, as either would directly degrade primary science data quality, while SR1 is the primary schedule-driver risk given the mission's demanding observation cadence.

6.4 Descope options

Two descope options are identified, should schedule, cost, or technical margins be threatened, each traded against its impact on science return.

1. **Reduce the number of target stars** (relaxes SR-006). Fewer targets reduce the total integration time required, easing schedule pressure, but at the cost of statistical significance across the stellar sample — weakening the population-level conclusions the mission is designed to deliver.
2. **Omit Mg II absorption-line resolution** (relaxes SR-20, SR-21). Without resolving the Mg II line, interstellar absorption cannot be corrected for, so stellar flux cannot be estimated correctly; this in turn prevents accurate EUV flux calibration and precludes atmospheric escape prediction without significant error. This descope is therefore only considered as a last resort, as it directly compromises the mission's primary science goal.

Both options are evaluated against their effect on science return and science closure, and their effect on mission operations, before being invoked.

6.5 Schedule

Table 22: *Key programmatic milestones.*

Milestone	Date	Note
Phase 0/A	2026–2031	Phase 0 (1 yr, from 2026) followed by Phase A/B1 (3–4 yrs); Mission Selection gate in 2027.
PDR	∼2033	Nominally closes Phase A/B1 at Mission Adaptation, ahead of Phase B2/C/D (7–8 yrs).
CDR	∼2037	Falls within Phase B2/C/D
Launch	2039	End of Phase B2/C/D.
End of mission	2049	End of nominal (5 yrs) + extended (+5 yrs) Phase E; Deorbit, followed by Phase F (<5 yrs, per ESSB-ST-U-007).

The schedule places PDR at the Phase B1–B2/C/D transition and launch in 2039, roughly 13 years after Phase 0 starts in 2026 – consistent with framing this as a compressed ESA

Phase 0–A study feeding directly into an M-class development timeline.

7 Conclusion

ICARUS will close the FGK-star ultraviolet survey gap left by the MUSCLES survey and its extension by tracing Ly-α, Mg,II, and NUV continuum emission, together with their short-term variability, across a sample of 435 nearby FGK stars spanning a wide range of stellar ages within 30 pc. The mission will employ a 0.5,m space telescope equipped with four spectrographs, providing spectral resolutions of up to $R \sim 115{,}000$, from a 600–800,km Sun-synchronous terminator orbit launched aboard Vega-C. The mass budget closes with ~49% margin against the launcher capability and the power budget closes with the Science mode as the sizing case at ~903 W against ~913 W EOL generation, within a ~900 M€ rough-order cost estimate. The total survey duration will add up to nearly five years. ICARUS will provide the scientific community with the first ever ultraviolet spectroscopic measurement of a systematically mapped, statistically significant, age-resolved sample of FGK-stars.

8 Acknowledgements

The whole team of the ICARUS mission wants to thank the organizers and sponsors of the Alpbach Summer School 2026 for the opportunity to take part in this educational program. Also, we are very thankful for the great support of our team tutors, Aljona Blöcker from the IWF and Christian Gritzner from the DLR as well as for the assistance of all roving tutors and lecturers present at the Summer School. We enjoyed working on our program very much and are proud of the effort every single team member put into this project.

References

[1] AZUR SPACE Solar Power GmbH. DB 00010891-01. Issued 11 April 2025; BOL efficiency 29.5–29.8% ("30% class"). AZUR SPACE Solar Power GmbH. 2025. URL: https://www.azurspace.com/media/uploads/file_links/file/bdb_00010891-01-00_tj3g30-advanced_4x8.pdf.

[2] A. Baglin et al. In: *36th COSPAR Scientific Assembly.* Vol. 36. Jan. 2006, p. 3749.

[3] Bradford Space. https://www.bradford-space.com/products/rwu. Commercial spacecraft attitude control subsystem product page describing Reaction Wheel Units, specifications, and flight heritage. 2025.

[4] Bradford Space. Product page. 2026. URL: https://www.bradford-space.com/products/rwu.

[5] A. P. Buccino and P. J. D. Mauas. In: 483.3 (June 2008), pp. 903–910. DOI: 10.1051/0004-6361:20078925. arXiv: 0804.1101 [astro-ph].

[6] Hongjing Cao et al. "Regional high-precision optical localization via scalable effective PSF modeling". In: *Measurement* 284, 122263 (Aug. 2026), p. 122263. DOI: 10.1016/j.measurement.2026.122263.

[7] C. Catala and Plato Team. In: *The CoRoT Mission Pre-Launch Status - Stellar Seismology and Planet Finding.* Ed. by M. Fridlund et al. Vol. 1306. ESA Special Publication. Nov. 2006, p. 497.

[8] Mark W. Claire et al. In: 757.1, 95 (Sept. 2012), p. 95. DOI: 10.1088/0004-637X/757/1/95.

[9] DHV Technology. PDF is image-based; specifications not independently extractable as text. DHV Technology. 2017. URL: https://dhvtechnology.com/wp-content/uploads/2017/05/DHV-Datasheet-Product-Space-Apr-17-web-1.pdf.

[10] DM Photonics. *Microchannel Plates and MCP Detectors and Imaging Systems – MCP References.* Accessed: 2026-07-22. 2026.

[11] Lincoln L. Endelman. In: *21st International Congress on: High-Speed Photography and Photonics.* Ed. by Ung Kim, Joon-Sung Chang, and Seung-Han Park. Vol. 2513. International Society for Optics and Photonics. SPIE, 1995, pp. 1204–1217. DOI: 10.1117/12.209584. URL: https://doi.org/10.1117/12.209584.

[12] European Space Agency. https://www.cosmos.esa.int/documents/332006/563627/xmm35.pdf. Technical documentation describing XMM-Newton spacecraft and detector systems, including thermal stabilisation heritage. 2000.

[13] European Space Agency. ESA Technical Note Issue 1, Revision 3. Approved version dated 15 June 2012. Noordwijk, The Netherlands: European Space Agency, June 2012. URL: https://sci.esa.int/documents/34375/36249/1567260131067-Margin_philosophy_for_science_assessment_studies_1.3.pdf.

[14] European Space Agency. *NewAthena.* ESA Science Programme. ESA flagship X-ray observatory; rescoped from Athena, approved 8 Nov 2023; L1 orbit; instruments WFI and X-IFU. 2026. URL: https://www.science.esa.int/web/cm25/newathena (visited on 07/22/2026).

[15] European Space Agency. *Plato.* ESA Science & Exploration. ESA Cosmic Vision M3 mission; 26 cameras; launch planned late 2026; L2 orbit. 2026. URL: https://www.esa.int/Science_Exploration/Space_Science/Plato (visited on 07/22/2026).

[16] European Space Agency. *Vega-C.* Mission page. Fairing: 3.3 m diameter, over 9 m tall. 2026. URL: https://www.esa.int/Enabling_Support/Space_Transportation/Vega/Vega-C.

[17] Kevin France et al. In: 820.2, 89 (Apr. 2016), p. 89. DOI: 10.3847/0004-637X/820/2/89. arXiv: 1602.09142 [astro-ph.SR].

[18] Kevin France et al. "The MUSCLES Treasury Survey. I. Motivation and Overview". In: *The Astrophysical Journal* 820.2 (2016), p. 89. DOI: 10.3847/0004-637X/820/2/89.

[19] Kevin France et al. "The Ultraviolet Radiation Environment around M Dwarf Exoplanet Host Stars". In: *The Astrophysical Journal* 763.2 (2013), p. 149. DOI: 10.1088/0004-637X/763/2/149.

[20] Gaia Collaboration et al. In: *Astronomy & Astrophysics* 674 (2023), A1. DOI: 10.1051/0004-6361/202243940.

[21] GomSpace A/S. https://gomspace.com/wp-content/uploads/2025/09/gs-ds-NanoMind_HP_MK3_DS_-_1036210_-_1_-_31_-_1.pdf. Technical datasheet for a high-performance spacecraft on-board computer based on the Xilinx Zynq-7000 programmable SoC platform. 2025.

[22] ICO Optics. Accessed: 2026-07-22. 2026.

[23] International Astronomical Union. IAU Scientific Bodies. Commission page describing the scope of IAU Com-

mission E2, covering solar magnetic activity, sunspots, flares, and coronal mass ejections. International Astronomical Union, 2025. URL: https://www.iau.org/CommissionE2/CommissionE2/Home.aspx (visited on 07/22/2026).

[24] Larson W. J. and Wertz J. R. In: (1992).

[25] Kosmolab / Syrlinks. Accessed: 2026-07-22. 2026.

[26] Michael W. McElwain et al. “Habitable World Discovery and Characterization: Coronagraph Concept of Operations and Data Post-Processing”. In: *Astronomical Society of the Pacific Conference Series*. Ed. by Janice C. Lee et al. Vol. 543. Astronomical Society of the Pacific Conference Series. Nov. 2026, p. 165.

[27] Kirpal Nandra et al. In: *arXiv e-prints*, arXiv:1306.2307 (June 2013). DOI: 10.48550/arXiv.1306.2307.

[28] NASA. *NASA Exoplanet Archive*. URL: https://exoplanetarchive.ipac.caltech.edu/ (visited on 07/21/2026).

[29] NASA Science. *About Hubble*. NASA Science. 2022. URL: https://science.nasa.gov/mission/hubble/overview/about-hubble/ (visited on 07/22/2026).

[30] NASA Science. *Fine Guidance Sensors*. Accessed: 2026-07-22. 2026.

[31] NASA Science. *Habitable Worlds Observatory*. NASA Astrophysics Division. Top-priority flagship mission concept from the Astro2020 Decadal Survey; successor to LUVOIR/HabEx studies. 2026. URL: https://science.nasa.gov/astrophysics/programs/habitable-worlds-observatory/ (visited on 07/22/2026).

[32] NASA Science. *IUE*. NASA Science. International Ultraviolet Explorer, 115–325 nm spectroscopy, operated 1978–1996. 2025. URL: https://science.nasa.gov/mission/iue/ (visited on 07/22/2026).

[33] NASA Science. *Neil Gehrels Swift Observatory*. NASA Goddard Space Flight Center. Launched 20 November 2004; three instruments: BAT, XRT, UVOT. 2026. URL: https://swift.gsfc.nasa.gov/ (visited on 07/22/2026).

[34] P. Odert et al. In: *International Journal of Astrobiology* 9.4 (Oct. 2010), pp. 239–243. DOI: 10.1017/S1473550410000315.

[35] Sarah Peacock et al. In: 170.5, 293 (Nov. 2025), p. 293. DOI: 10.3847/1538-3881/ae0a2f. arXiv: 2509.08999 [astro-ph.SR].

[36] RC Optical Systems. *Telescopes Overview*. Accessed: 2026-07-22. 2026.

[37] Ignasi Ribas et al. In: 622.1 (Mar. 2005), pp. 680–694. DOI: 10.1086/427977. arXiv: astro-ph/0412253 [astro-ph].

[38] Safran (formerly Syrlinks). Product page. Formerly hosted as Syrlinks EWC27 on kosmolab.space; original URL is dead (404). Developed jointly with CNES. 2026. URL: https://www.safran-group.com/products-services/x-lite-x-band-transmitter-nano-satellites.

[39] Sodern. https://sodern.com/en/ranges/hydra. Manufacturer product documentation for the Hydra modular star tracker used in spacecraft attitude determination systems. 2025.

[40] Sodern. Product page. Flight-proven since 2012, 245+ units launched. 2026. URL: https://sodern.com/en/ranges/hydra.

[41] J. P. Swings. In: *ESO Infrared Workshop*. Ed. by A. F. M. Moorwood and Kurt Kjaer. Jan. 1982, pp. 249–253.

[42] Teledyne Acton Optics. *Al+MgF2 Broadband Mirrors*. Accessed: 2026-07-22. 2026.

[43] Jennifer Wojno. Doctoral dissertation. Potsdam, Germany: University of Potsdam, 2017.

[44] Qirun Zhang et al. “Diffusion-based PSF priors for aberrated defocus correction”. In: *Optics Laser Technology* 203, 115791 (Nov. 2026), p. 115791. DOI: 10.1016/j.optlastec.2026.115791.